AUTHOR QUERY FORM

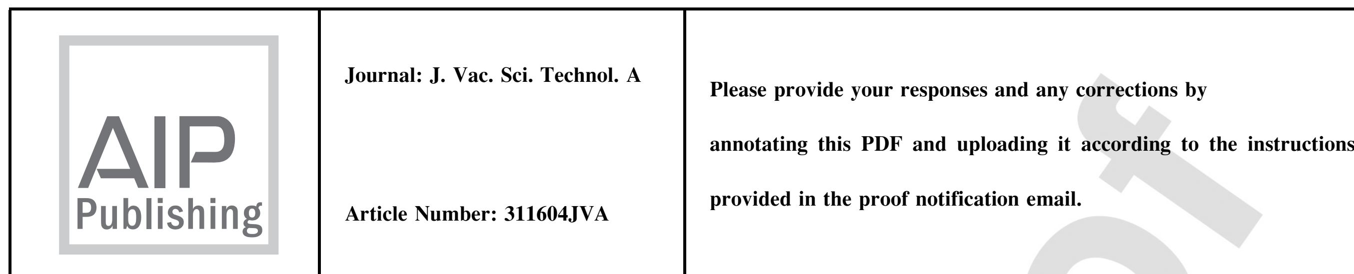

AIP Publishing	**Journal: J. Vac. Sci. Technol. A** **Article Number: 311604JVA**	**Please provide your responses and any corrections by annotating this PDF and uploading it according to the instructions provided in the proof notification email.**

Dear Author,

Below are the queries associated with your article; please answer all of these queries before sending the proof back to AIP.
Please indicate the following:
Figures that are to appear as color online only (i.e., Figs. 1, 2, 3) ____________________________(this is a free service).
Figures that are to appear as color online and color in print__________________(a fee of $325 per figure will apply).

Article checklist: In order to ensure greater accuracy, please check the following and make all necessary corrections before returning your proof.

1. Is the title of your article accurate and spelled correctly?
2. Please check affiliations including spelling, completeness, and correct linking to authors.
3. Did you remember to include acknowledgment of funding, if required, and is it accurate?

Checking details including author names and affiliations as well as Acknowledgments including grant numbers, etc. is important as Errata cannot be used for these type of minor edits once the article is online.

Location in article	Query / Remark: click on the Q link to navigate to the appropriate spot in the proof. There, insert your comments as a PDF annotation.
AQ1	Please check that the author names are in the proper order and spelled correctly. Also, please ensure that each author's given and surnames have been correctly identified (given names are highlighted in red and surnames appear in blue).
AQ2	Please define YAG at first occurrence.
AQ3	Please reword caption of Figs. 6, 8, 9, 13, 16 without color words, as readers of print will only see black and white figures.
AQ4	Please provide a digital object identifier (doi) for Ref(s). 12.

Thank you for your assistance.

Author Proof

PROOF COPY [JVSTA-A-16-161] 311604JVA

Defect formation during chlorine-based dry etching and their effects on the electronic and structural properties of InP/InAsP quantum wells

AQ1

Jean-Pierre Landesman[a)]
Institut de Physique de Rennes, CNRS-UMR 6251, Université Rennes 1, F-35042 Rennes, France

Juan Jiménez
GdS Optronlab, Dpto. Fisica de la Materia Condensada, Universidad de Valladolid, 47011 Valladolid, Spain

Christophe Levallois
UMR FOTON, CNRS, INSA-Rennes, 20 avenue des buttes de Coësmes, F-35708 Rennes, France

Frédéric Pommereau
III-V Lab, Route de Nozay, F-91461 Marcoussis, France

Cesare Frigeri
CNR-IMEM Istituto, Parco area delle Scienze 37/A, 43010 Parma, Italy

Alfredo Torres
GdS Optronlab, Dpto. Fisica de la Materia Condensada, Universidad de Valladolid, 47011 Valladolid, Spain

Yoan Léger and Alexandre Beck
UMR FOTON, CNRS, INSA-Rennes, 20 avenue des buttes de Coësmes, F-35708 Rennes, France

Ahmed Rhallabi
Institut des Matériaux Jean-Rouxel, CNRS-UMR 6502, Université Nantes 1, F-44322 Nantes, France

(Received 27 April 2016; accepted 3 May 2016; published xx xx xxxx)

The general objective is the investigation of the defects formed by dry etching tools such as those involved in the fabrication of photonic devices with III–V semiconductors. Emphasis is put on plasma exposures with chlorine-based chemistries. In addition to identifying these defects and describing their effects on the electro-optic and structural properties, the long-term target would be to predict the impact on the parameters of importance for photonic devices, and possibly include these predictions in their design. The work is first centered on explaining the experimental methodology. This methodology starts with the design and growth of a quantum well structure on indium phosphide, including ternary indium arsenide/phosphide quantum wells with graded arsenic/phosphor composition. These samples have then been characterized by luminescence methods (photo- and cathodoluminescence), high-resolution transmission electron microscopy, and secondary ion mass spectrometry. As one of the parameters of importance in this study, the authors have also included the doping level. The samples have been exposed to the etching plasmas for "short" durations that do not remove completely the quantum wells, but change their optical signature. No masking layer with lithographic features was involved as this work is purely oriented to study the interaction between the plasma and the samples. A significant difference in the luminescence spectra of the as-grown undoped and doped samples is observed. A mechanism describing the effect of the built-in electric field appearing as a consequence of the doping profile is proposed. This mechanism involves quantum confined Stark effect and electric-field induced carrier escape from the quantum wells. In the following part, the effects of exposure to various chlorine-based plasmas were explored. Differences are again observed between the undoped and doped samples, especially for chemistries containing silicon tetrachloride. Secondary ion mass spectrometry indicates penetration of chlorine in the structures. Transmission electron microscopy is used to characterize the quantum well structure before and after plasma bombardment. By examining carefully the luminescence spectral properties, the authors could demonstrate the influence of the etching plasmas on the built-in electric field (in the case of doped samples), and relate it to some ionic species penetrating the structures. Etching plasmas involving both chlorine and nitrogen have also been studied. The etching rate for these chemistries is much slower than for some of the silicon tetrachloride based chemistries. Their effects on the samples are also very different, showing much reduced effect on the built-in electric field (for the doped samples), but significant blue-shifts of the luminescence peaks that the authors attributed to the penetration of nitrogen in the structures. Nitrogen, in interstitial locations, induces mechanical compressive stress that accounts for the blue-shifts. Finally, from the comparison between secondary ion mass spectrometry and luminescence spectra, the authors suggest some elements for a general

[a)]Electronic mail: jean-pierre.landesman@univ-rennes1.fr

ID: aipepub3b2server Time: 16:07 I Path: D:/AIP/Support/XML_Signal_Tmp/AI-JVA#160068

Author Proof

J_ID: JVTAD6 DOI: 10.1116/1.4950445 Date: 11-May-16 Stage: Page: 2 Total Pages: 15
PROOF COPY [JVSTA-A-16-161] 311604JVA

mechanism involved in the etching by chloride-chemistries, in which a competition takes place between the species at the surface, active for the etching mechanism, and the species that penetrate the structure, lost for the etching process, but relevant in terms of impact on the electro-optic and structural features of the exposed materials. © *2016 American Vacuum Society*.
[http://dx.doi.org/10.1116/1.4950445]

I. INTRODUCTION

The semiconductor equipment industry has developed over the years a number of tools and processes which are today used at very large scales in fabrication throughout the world. Dry etching, also designated as reactive ion etching (RIE) or plasma etching, is one of these tools for the fabrication of ultralarge scale integrated circuits in the silicon microelectronics industry as well as in the fabrication of photonic integrated circuits with compound semiconductors based on gallium arsenide (GaAs) or indium phosphide (InP). It is used, in particular, to precisely define features with submicron dimensions, for example, transistor gates in the silicon world.[1] Very deep features, such as "through silicon vias," are also realized using different RIE setups.[2] The reactive source gases used in plasma etching of silicon are usually molecules containing fluorine atoms, while chloride or bromide based plasmas are mainly used for the etching of III–V semiconductor compounds like GaAs or InP.

Plasma etching is considered a mature technology. Nevertheless, research and development efforts on this technique are going on in a large number of places, both academic and industry centers, to adapt the processes and equipment to the challenges occurring constantly on the different roadmaps, both for silicon devices and III–V compound semiconductor devices. For example, pushing the limits of the "more Moore" approach for CMOS technologies requires plasma etching processes allowing gate design for the next technology nodes, etching of materials newly introduced into the gates, better control of the gate dimensions, etc.[3] As far as compound semiconductor device technologies are concerned, the trend to reduce critical dimensions—especially for plasma etching operations—seems less emphasized, the efforts being rather focused on developing plasma etching processes applicable to a wide variety of materials which are nowadays introduced in the devices. However, some devices also require plasma etching processes which can generate features with critical dimensions in the nanometer range and/or aspect ratios difficult to achieve (good examples of such devices are the optic or opto-electronic components based on photonic crystals).

Developing plasma etching processes involves research in different directions:

(1) plasma physics and chemistry, as well as reactor technology (for the part related to design of equipment);
(2) study of the plasma/surface interaction for each specific material;
(3) accurate metrology for the optimization of the expected features; this is mainly performed using electron microscopy;
(4) materials and device physics to check the overall compatibility of the plasma process with device performances.

In this paper, we explore the last direction, with a focus on plasma etching of InP-based structures. We investigate the effects of dry etching on the etched materials. We chose processes commonly used in the photonic device industry for etching InP and related materials (in our case, the reactive source gases are chlorine-based mixtures with either $SiCl_4$ or Cl_2). In the present stage of the study, our goal is to identify the mechanisms by which the reactive gases interact with the material. No specific geometric feature is designed at this stage of the study. We simply expose the material to the gases, under the conditions typically occurring during plasma etching, and thereafter, we analyze the changes induced in the materials using different experimental techniques. Therefore, the issues concerning the etching mask materials and design are not considered, but will be the object of forthcoming work.

The methodology involves the design of heterostructures which incorporate specific features [quantum wells (QWs)], role of which is to provide an in-depth signature of the effects induced by the etching gases, through changes in their luminescence spectral parameters. This is an approach used for a long time by groups trying to understand the effects of energetic ions or reactive radicals on compound semiconductors. The first studies on this topic were reported for GaAs and InP.[4,5] These pioneer studies dealt with the effects of ion bombardment (mainly rare gas ions) on samples with AlGaAs QWs in GaAs or GaInAsP QWs in InP. It was demonstrated that under the effect of ion bombardment even at low energy (400–500 eV or even lower), defects are produced at depths in the order of 100 to a few hundred nanometers. Channeling was proposed as the mechanism generating these defects.[6] Even if the ion bombardment experiment is not performed along directions where channeling is expected [e.g., etching (100) surfaces of GaAs or InP does not involve ion bombardment along a major channeling direction in these crystals], the fact that a very small fraction of the incident ions end-up travelling the crystal along other directions such as ⟨110⟩ can lead to this depth of penetration, and therefore promote the creation of defects across the structure. In these early studies, occurrence of defects at a specific depth below the surface is assumed from the reduction of photoluminescence (PL) efficiency of the QW located at such specific depth. From these investigations, the authors showed that ion bombardment experiments simulating the conditions occurring during plasma etching affect the materials on depths much larger than 100 nm, even when the ions energy lies between 100 and 500 eV. However, studying the effects of rare gas ions does not allow for the extrapolation to the case of industrial plasma etching processes. At least one paper reports on similar studies involving chlorine atomic and molecular ions derived from the decomposition

ID: aipepub3b2server Time: 16:07 I Path: D:/AIP/Support/XML_Signal_Tmp/AI-JVA#160068

scheme expected for $SiCl_4$ inside a RIE reactor.[7] Again, the decrease in PL yield from the QW is seen to extend deeper than 100 nm.

Similar experiments could not be carried out for the etching of Si, since there is no simple QW structure (with an efficient PL) that could be grown by epitaxy on Si. However, a fundamental paper was published by Winters and collaborators,[8] where the authors demonstrated the penetration of fluorine into the Si lattice under conditions that simulate the exposure to etching plasmas. The measurements, performed using x-ray photoelectron spectroscopy, demonstrated a penetration depth of at least 20 nm, but the actual depth of penetration could be larger (the technique used in this study does not allow the probing of larger depths).

Our aim in this study is to establish a scheme for the interaction of the ions penetrating during the process of exposure to the RIE plasma and the semiconductor materials under consideration (InP/InAsP). It is clear from the published results that this interaction leads to the creation of defects accounting for the reduction of the PL yield. However, the detailed mechanisms have not yet been described. The penetrating ions can have an impact on the electronic properties, both the charge carrier lifetime and the radiative recombination rate. The approach followed consists in analyzing all the PL spectral properties affected by the RIE process, and to use samples with similar design of the QW structure but different doping profiles (in order to see if the presence of internal built-in electric fields affects the response to the RIE plasma). Additional characterizations are used to complete the investigations: secondary ion mass spectrometry (SIMS) to probe directly the penetration of chlorine and transmission electron microscopy (TEM) to assess accurately the etch depths through the QW structure and also to check the crystal and QW interfaces quality. In a preliminary paper,[9] reporting our first results for exposure of the InP/InAsP samples to different chlorine-based plasmas, we have shown evidence of the chlorine penetration in parallel with significant modifications of the PL and cathodoluminescence (CL) spectra. The present paper describes the extensive study that we have performed along the general objective stated above.

II. EXPERIMENT

We first describe here the design and growth of the InP/InAsP heterostructure samples. In a second part, we explain the conditions for the RIE process. Finally, we give the necessary details on the conditions which have been used for the examination of the samples before and after exposure to the RIE plasmas.

A. Sample structure and growth

The QW structures were grown on n-doped (100) InP substrates (doping level: $10^{18}\,cm^{-3}$). The whole structure contains nine QWs. QW thickness is constant for each sample (7–10 nm). The QWs are made of $InAs_xP_{1-x}$ (with InP barriers), with As composition "x" graded along the QW series. In order to avoid reabsorption of the PL, the QW with the smallest energy bandgap (highest As content) was grown deepest—i.e., closest to the substrate—while the QW with the highest As content was grown closest to the sample surface. Typical values for x (As composition) are between 0.35 (QW closest to the surface) and 0.49 (deepest QW). A buffer layer (400 nm InP) is first grown prior the QW series. The InP barrier thickness is 100 nm. An InP cap (300 nm) is finally grown after the last QW. The different QWs will be denoted as QW 1 to QW 9 (from surface to bulk). Therefore, the bandgap energy decreases from QW 1 to QW 9.

Figure 1 gives a schematic picture of this structure.

The samples were grown by gas source molecular beam epitaxy, using AsH_3 and PH_3 precursors, and a solid source for In. The layers could be grown either nonintentionally doped, or with Si or Be dopants for n-type and p-type, respectively. Two different samples will be investigated here:

(1) Sample 1 was grown without intentional doping.
(2) Sample 2 was doped: n-type ($1 \times 10^{18}\,cm^{-3}$) for the InP buffer layer, and p-type ($7 \times 10^{17}\,cm^{-3}$) for the InP barrier and cap layers. QWs were not intentionally doped.

B. Reactive ion etching

Commercial inductively coupled plasma RIE systems were used. These reactors have two RF power sources: one for the plasma excitation, and one for the control of the bias at the substrate.[10] For the present study, we focused on different etching processes available at III–V Lab for the fabrication of InP-based photonic devices. No specific process was designed for the experiments carried here. Three different etching chemistries were investigated, with the parameters described in Table I.

Etching rates differ strongly from one process to the other and will be estimated from the SIMS measurements and TEM images. The first process ($SiCl_4/H_2/Ar$) produces an etch rate in the order of 500 nm/min. The Cl_2/N_2 process with the conditions above was chosen for its very low etch

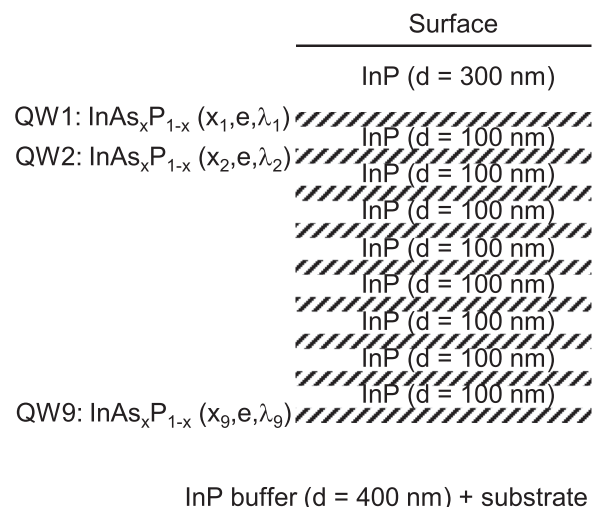

FIG. 1. QW structure used for the study. x denotes the As composition for each QW, e the QW thickness, and λ its corresponding PL wavelength.

ID: aipepub3b2server Time: 16:07 I Path: D:/AIP/Support/XML_Signal_Tmp/AI-JVA#160068

TABLE I. Plasma parameters used for the three different etching chemistries investigated.

Etching chemistry	Gas flow rates	Total pressure	RF power plasma excitation	RF power sample stage	Sample bias
$SiCl_4/H_2/Ar$	5 sccm $SiCl_4$/2 sccm H_2/10 sccm Ar	5 mTorr	1200 W	250 W	60 V
Cl_2/N_2	3 sccm Cl_2/20 sccm N_2	5 mTorr	900 W	25 W	30 V
$SiCl_4/Ar$	4 sccm $SiCl_4$/5 sccm Ar	5–10 mTorr	1000–1200 W	110–350 W	40–90 V

rate. The third process ($SiCl_4/Ar$) was adjusted to provide different etch rates with the same chemistry.

The temperature at sample surface during etching was estimated using temperature labels. This estimation showed that the surface temperature is always below 200 °C for the conditions of the present study. Care was taken to wait long enough for stationary operation of the reactor during the temperature estimates. Such temperature rise is far from the threshold for atom diffusion in InP-based materials. Therefore, no cooling of the samples was provided.

C. Photoluminescence and cathodoluminescence

The PL experiments were performed at 15 K, with 1064 nm YAG laser excitation. This energy is below the band gap of InP substrate and barriers (thus avoiding excitation in these parts of the structure). Excitation power density was in the range of few hundreds to 1000 W/cm^2. The standard excitation power density for the spectra presented in this paper is 500 W/cm^2. This power density is slightly higher than standard PL excitation (~100 W/cm^2), but since the barriers are transparent at the pump wavelength, only a small fraction of this power is absorbed by the nine QWs. Furthermore, we checked that all the PL experiments have been conducted in a linear absorption regime and at a low excitation power.

For the CL measurements, we used a Carl Zeiss (LEO 1530) field emission scanning electron microscope, equipped with a Gatan mono-CL2 system with a cooled nitrogen InGaAs array detector. The acceleration voltage for the electrons was set to 20 kV [which gives a penetration depth for InP in the order of 1 μm (Ref. 11)]. The measurement temperature for CL spectra shown in this paper is systematically 80 K.

D. Transmission electron microscopy

TEM observations were made in a field emission gun JEOL 2200FS machine working at 200 keV under different operation modes:

(1) High resolution TEM (HRTEM). This is the usual mode to get atomic resolution of the sample, allowing, for example, the investigation of the QW interfaces quality.
(2) High angle annular dark field (HAADF) which, in association with the scanning operation mode of the TEM (STEM), allows getting information on the composition of each layer, thanks to the Z^2 dependence of the HAADF intensity, with Z the atomic number.[12]
(3) High resolution scanning TEM, where atomic resolution can in principle be coupled with contrast related to the local chemical composition.

Sample preparation for the TEM observations was done by standard thinning by Ar^+ ion bombardment of cross sectional samples, whose thickness had been previously reduced by mechanical grinding. To avoid decomposition of the samples as much as possible, these were kept at liquid nitrogen temperature during the Ar^+ ion thinning process.

E. Secondary ion mass spectrometry

SIMS profiles were produced by Cs^+ primary ion bombardment at 16 keV. The secondary species detected were Cl (mass 35), P_2 (mass 31), and As (mass 75). We did not perform any kind of calibration to evaluate absolute atomic concentrations. However, quite reproducible signals for P and As were obtained from sample to sample (around 6% reproducibility for the P_2 signal from sample to sample, and 15% for the As signal). Based on the assumption that count rates with a similar magnitude are measured for the As and P profiles in different samples, we took the raw data for the Cl profile as a good indication of the actual Cl concentration profile, without performing any calibration. As for the depth scales and depth resolution of the SIMS profiles, no calibration was required since the samples include their own internal scales consisting in the series of nine InAsP QWs whose depth is known. The SIMS profiles are given as a function of sputter time by Cs^+ ions. The conditions for ion sputtering (ion energy, ion beam current) were kept constant for all the measured profiles. This ensures the possibility to directly compare the secondary ion signals from the different samples, assuming that the sputter yields for the different elements do not change from each other sample.

III. RESULTS

A. As-grown samples

Figure 2 shows the PL spectra recorded for the as-grown samples. The spectra for the two samples look very different, the PL lines being much broader on the doped sample. This is not related to the crystal quality, e.g., to the more or less abrupt character of the QW interfaces. The crystal quality was checked by the TEM observations, in particular high resolution TEM as illustrated on Fig. 3.

The CL spectra for the two samples are shown on Fig. 4. They display the same trend as the PL spectra, the difference in the shape of the luminescence lines being even more pronounced for the CL. In fact, on the CL spectrum of the doped sample [Fig. 4(b)], one can only distinguish eight peaks. Since the QWs themselves are not doped, we do not have a straightforward explanation for the observed difference. To investigate this, we performed some luminescence measurements on the samples under an electric bias. Our PL setup

Author Proof
ID: aipepub3b2server Time: 16:07 I Path: D:/AIP/Support/XML_Signal_Tmp/AI-JVA#160068

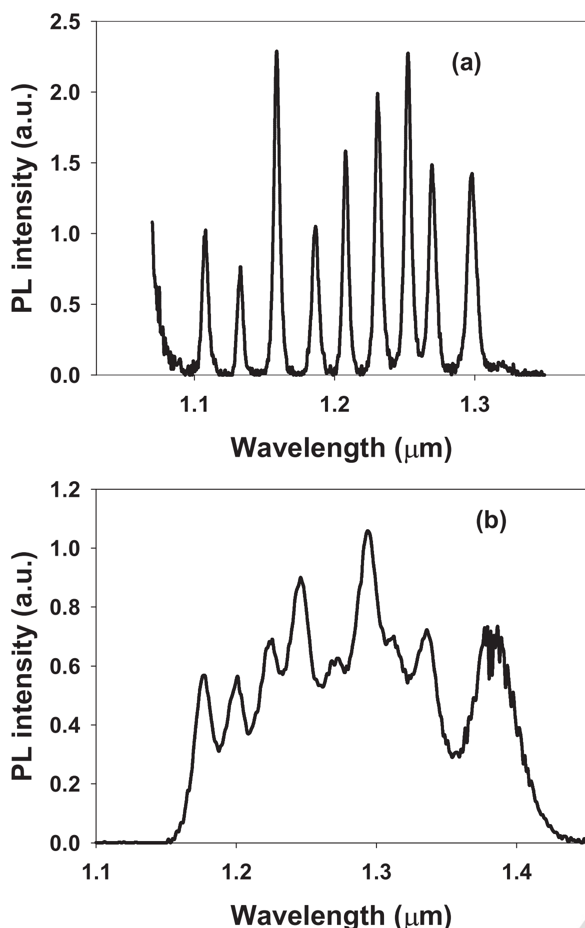

FIG. 2. PL spectra measured at 15 K with 1064 nm laser excitation of the as-grown samples: (a) Undoped sample and (b) doped sample.

did not allow biasing the sample; therefore, these measurements were performed with the CL setup only. The idea behind this investigation was to check the influence of the built-in electric field present in the samples (due to the doping profile) on the luminescence line shape. The electric field can induce a quantum confined Stark effect (QCSE) and can also move the photogenerated carriers away from the QW where they are generated.[13] These can strongly affect the PL line shape. QCSE can produce red-shift to longer wavelengths, lowering of the intensity, and spectral broadening.[13] Electric field-induced tunneling of the photogenerated carriers out of the QWs induces quenching of the PL.[13]

In order to probe these two effects (QCSE and luminescence quenching by electric field-induced tunneling), it is necessary, in principle, to start from the flat-band situation;[13] however, the band bending of our samples is complex:

(1) Sample 1 (grown nominally undoped) is nevertheless grown on a doped substrate (n-type).
(2) Sample 2 involves a p-n junction (at the transition between the buffer layer and QW 9). Thus, the electric field reaches its maximum at thermal equilibrium close to QW 9.

The Fermi level is most probably pinned at the surface[14] for both samples. Since the QW structure is grown very close to the surface, this Fermi level pinning also affects the distribution of the electric field across the structure. Therefore, it is quite difficult to assess how the electric field should change throughout the structure for different applied biases. For sample 1, we assumed that at thermal equilibrium the electric field is very low in the QWs region. For sample 2, we assumed that the maximum of the electric field occurs close to QW 9 because of the p-n junction. Without being able to determine the flat band situation, all we did was to observe the changes in the CL spectra as a function of the sample biasing, which was applied at the surface through a contact made of silver paste. The backside of the substrate was grounded. The CL measurements were made immediately next to the surface contact.

Figure 5 gives the results for the CL measurements under positive surface bias for both samples. For the undoped sample, this positive bias induces a red-shift and a quenching of the luminescence, especially at 3 V. We interpret this as an increase in the band-bending compared to the situation where no voltage is applied, and it can be attributed to the above mentioned QCSE. For the doped sample, there is no significant change up to 2 V (modifications of the CL

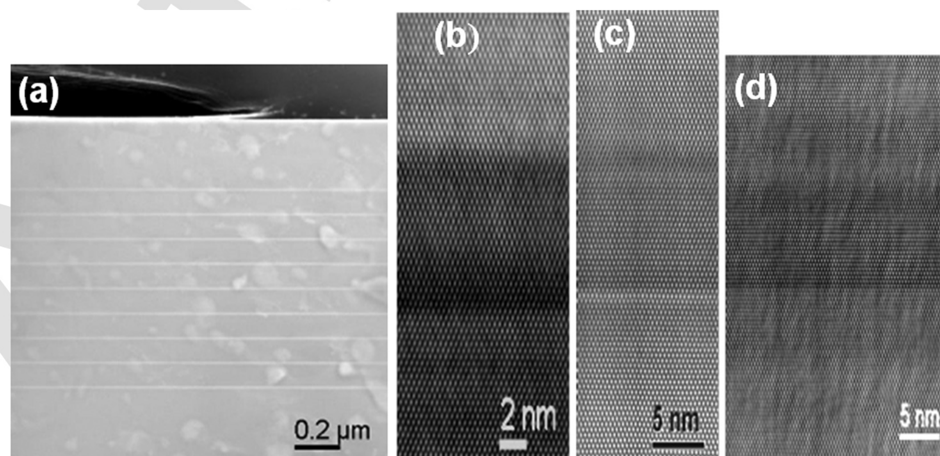

FIG. 3. TEM observations on the as grown doped sample. (a) HAADF image of the whole structure (the substrate is at the bottom). (b)–(d) HRTEM images of QW 9 (a), QW 8 (b), and QW 3 (c). Note that the magnification for these three images is different. The substrate is at the bottom also for the HRTEM images.

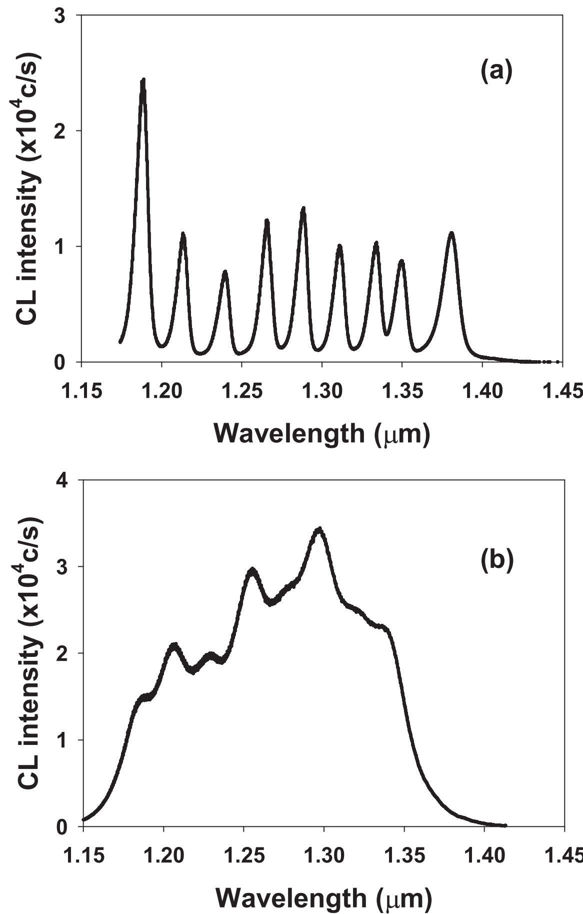

FIG. 4. CL spectra measured at 80 K of the as-grown samples: (a) undoped sample and (b) doped sample.

intensity observed for 0, 1, and 2 V are considered within the reproducibility limits of the CL setup). However, a drastic change starts at 3.2 V: QW 9, which was absent from CL spectra at lower voltage, increases, even dominating the CL emission at 5 V. A sharp line associated with QW 9, possibly made of two contributions, is observed at this voltage. We interpret this observation as evidence that the generated charge carriers were initially (at 0 V) completely driven out of QW 9 by the built-in electric field, resulting in the absence of the CL emission in QW 9. Above 3.2 V, the effective electric field at the p-n junction is reduced so that QW 9 starts being visible on the CL spectra. As for the other QWs, they are probably in a region where the band bending is not significantly modified by the applied bias, due to Fermi level pinning at the surface, and to the fact that the p-n junction absorbs most of the effects of the applied bias.

The difference in the response to surface positive bias of the CL spectra allows us to conclude that these spectra are strongly affected by the doping level through the QCSE and luminescence quenching by electric field-induced tunneling. Band bending in the undoped sample, at thermal equilibrium, is small, and thus, the PL and CL spectra display the intrinsic luminescence line spectra. In the doped sample, the presence of a p-n junction affects the spectra even at thermal equilibrium, in the sense that QW 9 is completely absent in the CL spectrum (although it is seen in the PL with an associated broad line), and all the other QWs produced a broadened luminescence line shape. The different observations for QW 9 on the CL and PL can be attributed to the difference in the excitation processes: due to the limited penetration depth of the electrons at 20 kV, this QW is more difficult to

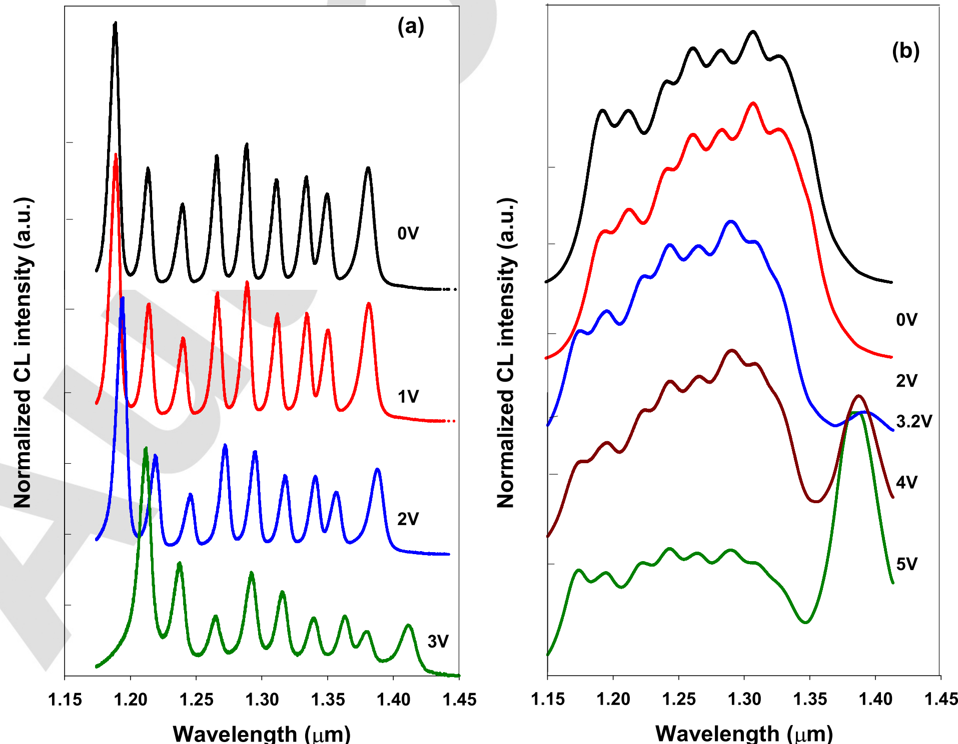

FIG. 5. (Color online) CL spectra as a function of the bias applied: (a) undoped sample and (b) doped sample.

excite than in the PL with 1064 nm excitation. From Ref. 11, it can be estimated that the number of electron-hole pairs generated by an incident electron with 20 kV kinetic energy decreases rapidly after a depth of 0.5 μm (although this paper deals with AlGaAs instead of InP, we can calculate a similar trend for our samples). On the other hand, 1064 nm corresponds to an energy below the band-gap for photons in InP, and thus, its penetration is much larger than the depth of the QW structure in our samples.

Finally, we also measured the SIMS profiles for the as-grown samples. Figure 6 gives an example of such a profile obtained on the doped sample. The surface peak observed for Cl is an effect of the very high sensitivity of the SIMS technique: the sample surface was contaminated by some Cl compound. However, we can see on Fig. 6 that the Cl profile drops to the background level after about 10 s sputtering. As for the P and As profiles, the QW structure is clearly identified. Figure 7 displays the As profile alone, where the qualitative correlation with the As content in the QW is seen (through an increasing background level between the deepest QWs).

B. $SiCl_4/H_2/Ar$ process

We now describe the results corresponding to the etching with the $SiCl_4/H_2/Ar$ plasma, first describing the PL and CL measurements, and then comparing with TEM and SIMS observations.

The $SiCl_4/H_2/Ar$ process was optimized especially with respect to the very fast etching rate. In the first set of experiments, the samples were exposed 1 min to this plasma to avoid the risk of a complete removal of the QW structure.

Figure 8 is a superposition of the PL data for the as-grown samples, and the samples exposed 1 min to the $SiCl_4/H_2/Ar$ plasma. Note that the two samples were not exposed in the same run. On the undoped sample, the signal for QW 1 and QW 2 has disappeared after exposure. On the doped-sample, only the signal for QW 1 disappeared.

The plasma takes a fraction of a minute to stabilize; therefore, 1 min is the shortest exposure that could be performed in a stationary regime; thus, we can expect slight differences

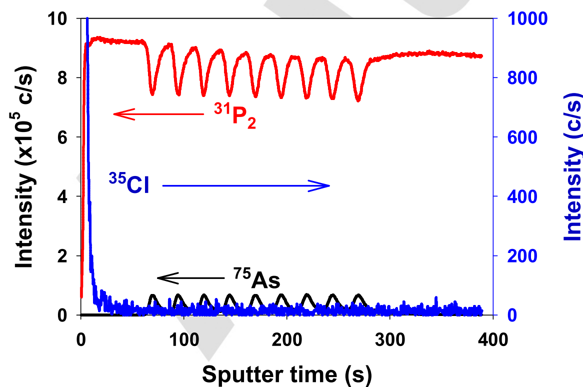

FIG. 6. (Color online) SIMS profiles measured on the as-grown, doped sample: $^{31}P_2$ (red), ^{75}As (black), and ^{35}Cl (blue). The scale on the left is for P and As, and the scale on the right is for Cl.

AQ3

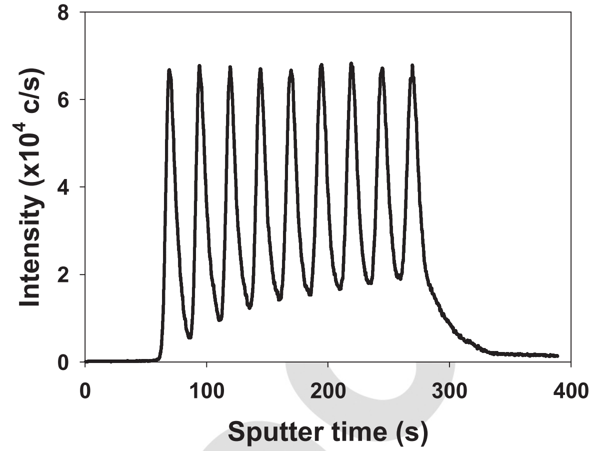

FIG. 7. SIMS profile measured on the as-grown, doped sample, for ^{75}As. This isolated profile is the same as that shown for ^{75}As in Fig. 6. It is displayed separately for clarity.

in the amount of etched material for two separate exposures, even if the nominal reactor parameters are the same.

Apart from the number of QWs having apparently been etched, there is another very significant difference. For the undoped sample, the remaining QWs have similar spectral characteristics to those of the corresponding QWs on the as-grown sample, except for a slight shift to shorter wavelength ("blue-shift") for QW 4, QW 6, and QW 8. For the doped sample, a pronounced sharpening of the luminescence peaks arising from QW 2 to QW 8 is observed; simultaneously, the peaks present a significant shift to the blue.

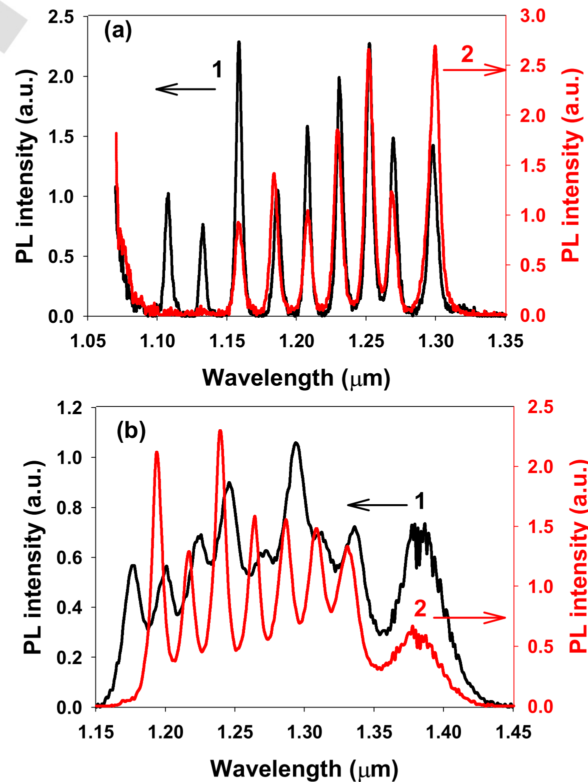

FIG. 8. (Color online) PL spectra of the samples as-grown (line in black) and exposed to the $SiCl_4/H_2/Ar$ plasma for 1 min (line in red): (a) undoped sample and (b) doped sample.

In order to specify more precisely the etching depth, we measured the SIMS profiles. As an example, Fig. 9 displays the results for the doped sample. The resolution of the profiles is disturbed, probably because of the roughening that occurs at the surface as the etching proceeds faster. Rough surfaces induce a loss of depth resolution during SIMS profiling. Anyhow, we can identify in Fig. 9 that the nine QWs are still present in the sample (there are nine clearly visible minima in the P profile, with the corresponding nine maxima on the As profile). To complete the scheme concerning the etch depth, we have performed a TEM observation of the same sample. This is shown in Fig. 10. From this image, we can estimate, by comparison with the image in Fig. 3, that 250 nm of the InP cap have been etched, but all the nine QWs remain present. Therefore, we can conclude at this stage that the PL yield of the QWs closest to the surface is completely reduced after plasma exposure, even if these QWs have not been etched at all. For the doped samples (where we have the SIMS and TEM information to compare), QW 1 is affected by the reduction. For the undoped sample (for which we have not performed SIMS and TEM), if we assume a similar etch depth, QW 1 and QW 2 were affected. It should be noted (for the undoped sample) that for the QWs remaining visible on the PL the peak intensity is much higher than the corresponding intensity on the same sample prior to etching.

The other information retrieved from the SIMS has to do with the Cl profile: after exposure to the $SiCl_4/H_2/Ar$ plasma for 1 min, it takes more than 50 s sputtering for the Cl signal to reach a background level slightly higher than for the as-grown sample. We deduce from this observation that some Cl has penetrated through the sample. This is best visualized in Fig. 11 where the Cl profiles for the as-grown sample and the samples exposed 1 min to the $SiCl_4/H_2/Ar$ plasma are represented on a log scale (sputtering from 0 to 100 s).

To complete this part on the 1 min exposure to the $SiCl_4/H_2/Ar$ plasma, the corresponding CL spectra measured on the same samples are shown in Fig. 12. For the undoped samples, we can notice that the magnitude of the changes is larger than for the PL measurements on the same samples. The changes for the CL yield must be related to the smaller probed depth for the 20 keV electrons than for the 1064 nm photons: after etching 250 nm of the InP cap layer, the deeper QWs become more efficiently excited. The blue-shift observed on the remaining QW transitions is more pronounced than the shift observed on the PL spectrum. This has to be related to the excitation process, different for PL and CL. For the doped sample, the most noticeable trends are the strong increase in QW 9 CL emission after exposure to the plasma, and the strong blue-shifts for the other QWs, which is coherent with what is observed on the PL spectra, although the shift is larger than the one measured by PL. The spectral sharpening seen especially for QW 2, QW 3, QW 4, QW 5, and QW 6 on the doped sample after exposure is also observed on the CL, something similar to the PL. This will be discussed with regard to the different band bending situations for the undoped and doped samples, and assumptions on the nature of the penetrating species.

Finally, for the case of the $SiCl_4/H_2/Ar$ plasma, the doped sample was also exposed for 2 min. We just show in Fig. 13 the PL, TEM, and SIMS data for this sample. Etching has

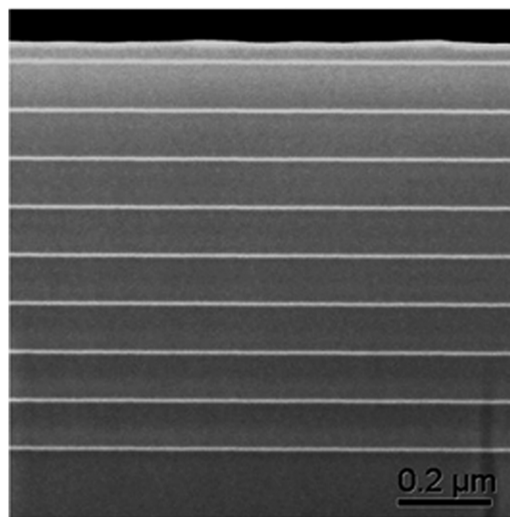

FIG. 10. HAADF image of doped sample after 1 min exposure to the $SiCl_4/H_2/Ar$ plasma.

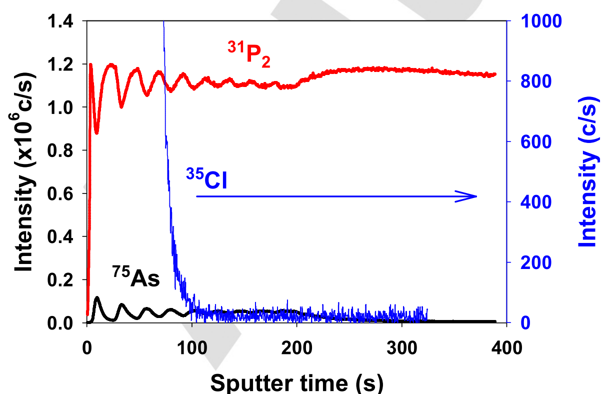

FIG. 9. (Color online) SIMS profiles measured on doped sample after 1 min exposure to the $SiCl_4/H_2/Ar$ plasma: $^{31}P_2$ (red), ^{75}As (black), and ^{35}Cl (blue). The scale on the left is for P and As, and the scale on the right is for Cl.

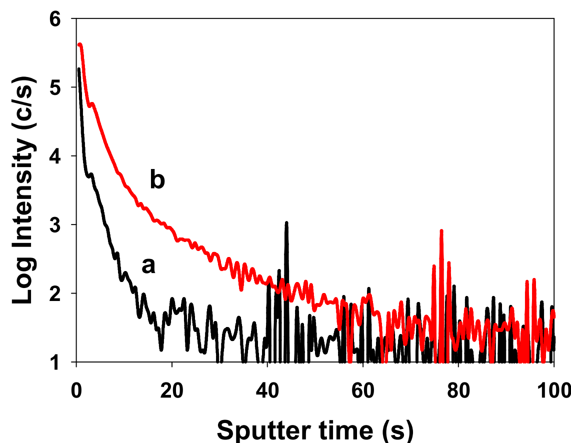

FIG. 11. (Color online) SIMS profiles measured on doped sample before (a) and after 1 min exposure to the $SiCl_4/H_2/Ar$ plasma (b) for ^{35}Cl on a log scale, for the early etching between 0 and 100 s.

ID: aipepub3b2server Time: 16:07 I Path: D:/AIP/Support/XML_Signal_Tmp/AI-JVA#160068

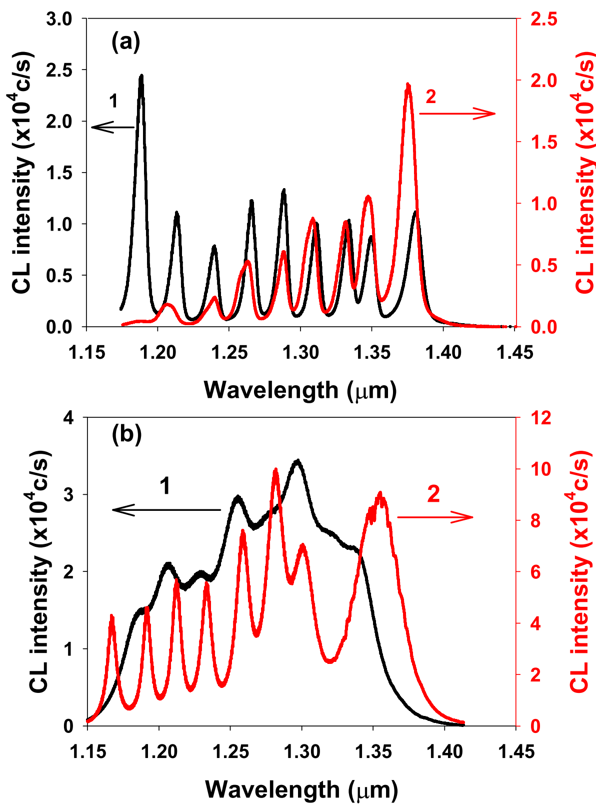

FIG. 12. (Color online) CL spectra of the samples as-grown (1) and exposed to the $SiCl_4/H_2/Ar$ plasma for 1 min (2): (a) undoped sample and (b) doped sample.

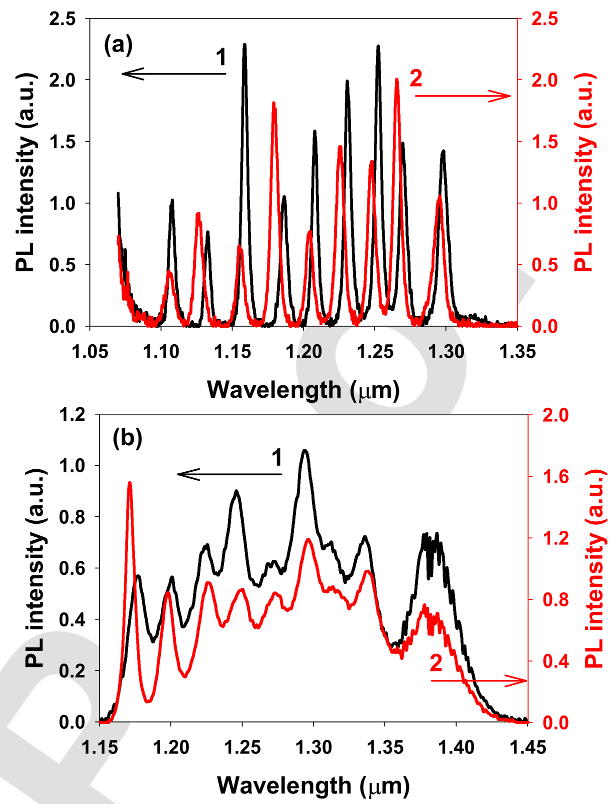

FIG. 14. (Color online) PL spectra of the samples as-grown (1) and exposed to the Cl_2/N_2 plasma (2). (a) Undoped sample, plasma exposure 4 min; (b) doped sample, plasma exposure 3 min.

stopped almost exactly at QW 4 (etch depth approximately 600 nm). QW 5, QW 6, QW 7, QW 8, and QW 9 still emit brightly on the PL spectrum. For these QWs, the transitions are significantly sharper (in terms of spectral width) than after 1 min exposure to the same plasma and the blue-shift appears increased.

C. Cl_2/N_2 process

The PL spectra for both the undoped and the doped samples (unfortunately, the duration of the plasma exposures differ—4 min in the first case, 3 min in the second case, but this will not block the discussion) are shown in Fig. 14. The first point to note is that even after 4 min etching, QW 1 has not been reached by the etching process, in agreement with the slower rate of this etching process (as compared to $SiCl_4/H_2/Ar$, at least under the conditions used in this work). Indeed, results from previous studies[15] show that dissociation and ionization processes of Cl_2 by electron impact are less efficient in Cl_2/N_2 plasmas because of the decrease in electron density with the percentage of N_2. The precise etch depth will be examined from the TEM images and SIMS profiles. The second point is that the PL yield is not at all affected by the Cl_2/N_2 exposure. This is in strong contrast with what was observed for $SiCl_4/H_2/Ar$ after 1 min and also with some published results. The third point, for the doped sample, is

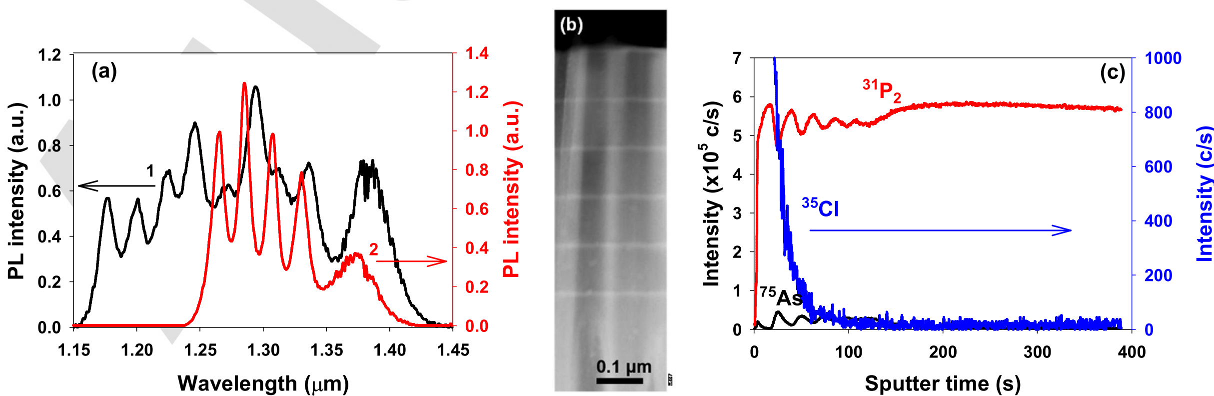

FIG. 13. (Color online) PL spectra (a), HAADF image (b) and SIMS profiles (c) of the doped sample exposed to the $SiCl_4/H_2/Ar$ plasma for 2 min. PL spectra of as-grown sample (1) and exposed sample (2). In the SIMS plot, red is for P, black for As, and blue for Cl.

554 that the Cl_2/N_2 exposure does not seem to affect very significantly the spectral shape of the QW transitions, except for QW 1 and maybe QW 2, whose associated luminescence bands appear sharper after exposure. The difference appears very important with the $SiCl_4/H_2/Ar$ exposure [Figs. 8(b)] where all the luminescence bands, except QW 9, were sharpened. Finally, concerning the undoped sample, we note that the blue-shifts are now observed for all QW transitions, the peak shift being larger than for the $SiCl_4/H_2/Ar$ exposure. Using a standard fitting procedure (using the Voigt profile, consisting of the convolution of a Lorentzian function by a Gaussian broadening, for each contribution) for PL experimental spectra, we could determine the following blue-shifts (Cl_2/N_2—exposed sample compared to as-grown sample), indicated on Table II. QWs 2, 4, and 6 have the maximum shifts. Let us recall that these shifts are much more pronounced than for the $SiCl_4/H_2/Ar$—1 min exposure [the corresponding values were estimated less than 2 nm for QWs 3–9 on Fig. 8(a)]. Fitting the PL spectra for the doped sample to extract accurate spectral shifts was not fully reliable because of the overlap between neighboring peaks.

A TEM-HAADF image of the doped sample after 3 min etching with Cl_2/N_2 is displayed in Fig. 15. InP cap layer of 120 nm still remain, while 180 nm were etched.

SIMS profiles for the doped samples exposed 1 and 3 min to the Cl_2/N_2 plasma are shown on Fig. 16. The Cl signal appears somewhat higher in the bulk part after 1 min than after 3 min, but this may be due to background contamination in the SIMS apparatus for this specific measurement.

D. $SiCl_4$/Ar process

This process was tested with the idea to investigate samples etched with a single process, but strongly different etch rates. In order to change the etch rate, the RF power at the plasma excitation source and at the sample biasing source were changed, keeping the flow rates for $SiCl_4$ and Ar constant. The total pressure in the plasma chamber was also adjusted. Slower etch rate was obtained by reducing the two RF powers (from 1200 to 1000 W at the plasma excitation stage and from 350 to 110 W at the sample stage), simultaneously increasing the total pressure (from 5 to 10 mTorr) in the plasma chamber (which helps decreasing the sample bias).

TABLE II. Spectral shifts estimated from the PL data for the undoped sample in Fig. 14(a).

Quantum well number	Spectral shift (nm)
QW 1	1.7
QW 2	7.2
QW 3	3.3
QW 4	6.2
QW 5	4.1
QW 6	5.6
QW 7	3.9
QW 8	3.9
QW 9	2.8

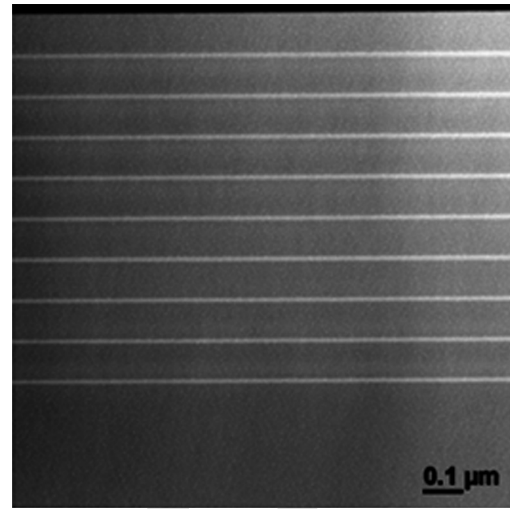

FIG. 15. HAADF image of doped sample after 3 min exposure to the Cl_2/N_2 plasma.

We could perform this part of the study only on the doped sample. We discuss below the CL spectra and SIMS profiles.

(1) $SiCl_4$/Ar slow etching process:

The results in Fig. 17 were obtained with plasma tuning (RF power, total pressure) to limit the etch rate. The sample bias was 40 V.

The main change on the CL spectra concerns QW 1, which displays a sharp and intense transition after plasma

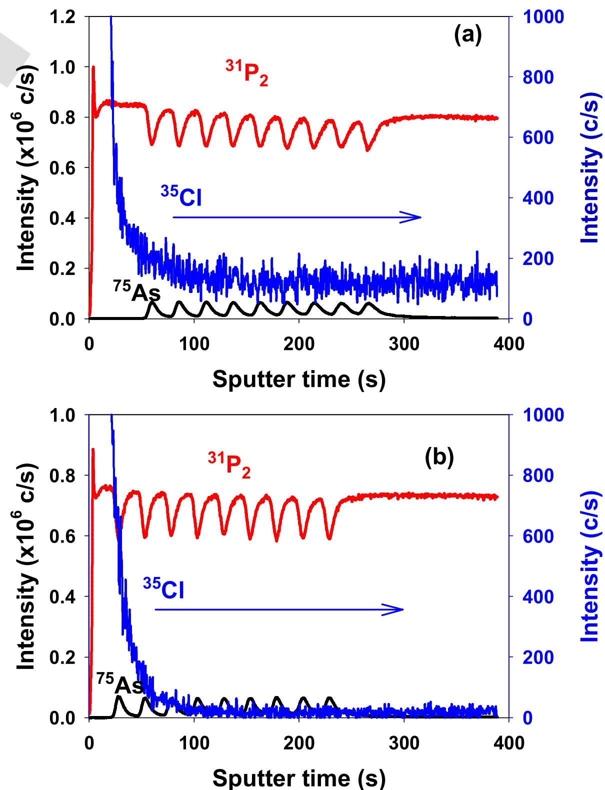

FIG. 16. (Color online) SIMS profiles measured on doped sample after 1 min (a) and 3 min (b) exposure to the Cl_2/N_2 plasma, respectively: $^{31}P_2$ (red), ^{75}As (black), and ^{35}Cl (blue). The scale on the left is for P and As, and the scale on the right is for Cl.

ID: aipepub3b2server Time: 16:07 I Path: D:/AIP/Support/XML_Signal_Tmp/AI-JVA#160068

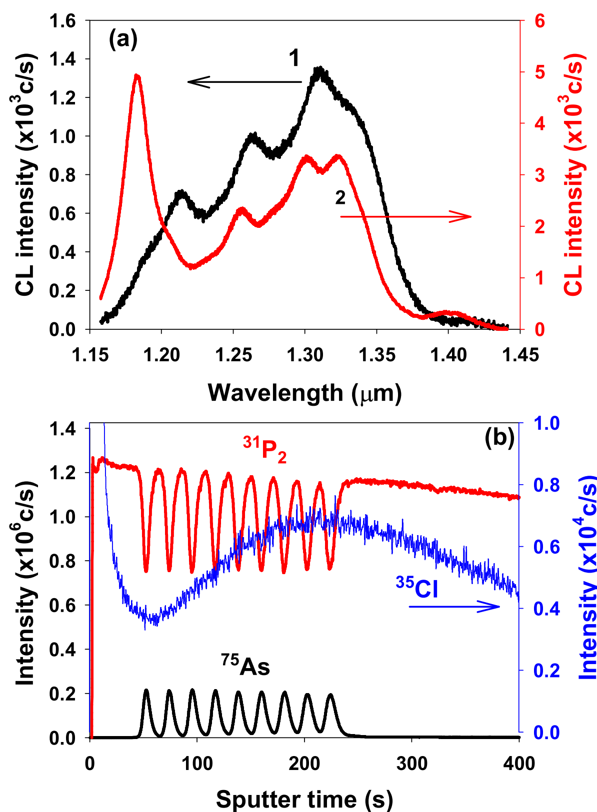

FIG. 17. (Color online) CL spectra (a) and SIMS profiles (b) for the doped-sample as-grown and exposed to the $SiCl_4$/Ar plasma—slow etching process (1 min). The spectrum (1) corresponds to the as-grown sample, and the spectrum (2) corresponds to the plasma exposed surface.

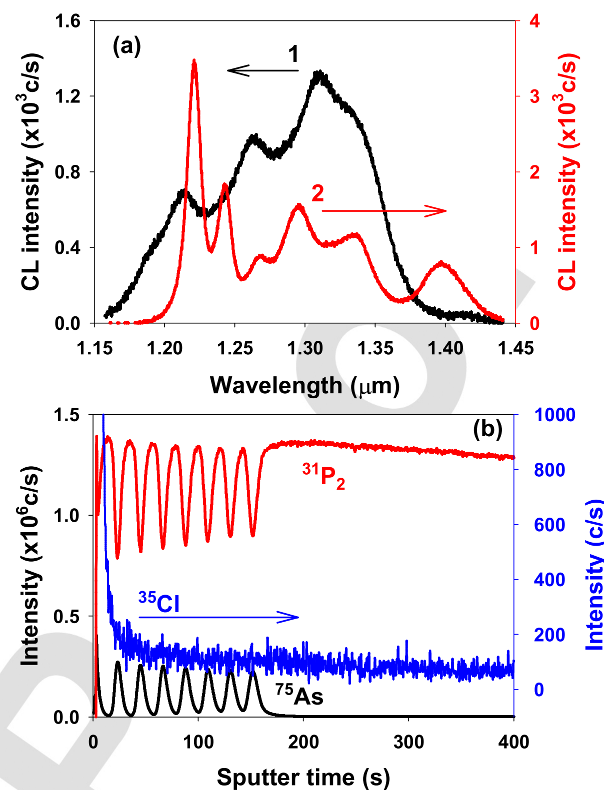

FIG. 18. (Color online) CL spectra (a) and SIMS profiles (b) for the doped-sample as-grown and exposed to the $SiCl_4$/Ar plasma—fast etching process (1 min). The spectrum (1) corresponds to the as-grown sample, and the spectrum (2) corresponds to the plasma exposed surface.

exposure. The other structures did not present relevant changes in the CL spectra. While QW 9 starts to become visible, the SIMS profiles tell us that the sample was almost not etched. They also indicate that the Cl signal has increased to about 7000 counts inside the sample after plasma exposure, compared to about 10–20 counts measured for the as-grown sample (cf Fig. 6). The Cl profile has a clear maximum at about 1 μm below the surface. The distribution of Cl inside the sample presents an implantationlike profile.

(2) $SiCl_4$/Ar fast etching process:

To measure the impact of the etch rate (keeping constant the $SiCl_4$ and Ar flow rates), the RF power for the plasma excitation and at the sample stage was increased. The sample bias reached 90 V. The corresponding results—CL spectra and SIMS profiles—are shown in Fig. 18, for a plasma exposure of 1 min.

The SIMS profiles show that the etching has reached QW 2 (etch depth: 400 nm). From the PL spectra, comparing with the spectra in Fig. 17, we conclude that the luminescence bands associated with QW 3 and QW 4 transitions have strongly sharpened, and their intensities have increased. The transitions for deeper QWs also evidence a beginning of sharpening.

From the SIMS data, we see that the Cl signal in the bulk is very low, we do not see any more the Cl signal obtained after the slow etching plasma.

IV. DISCUSSION

We suggest in this section a discussion of the results described in the previous paragraphs. The comparison between the behaviors of the undoped and doped samples under the same plasma exposures will be helpful to understand the changes induced by the plasma exposure in the two samples and the different etching procedures.

The $SiCl_4/H_2$/Ar plasma was first investigated. The etch rate with this plasma is 250 nm/min (and 600 nm/2 min; the deviation from linearity is due to the time necessary for the plasma to stabilize). After 1 min, we observe the luminescence of QW 1 completely suppressed (and even for QW 2 in the case of the undoped sample). However, only a part of the InP cap layer has been etched, meaning that the QWs themselves have not been etched. This suppression of the luminescence for the QWs closest to the surface is due to the diffusion of defects, probably Cl-related defects formed when Cl penetrates the structure below the surface, as shown by the SIMS profiles. This result keeps resemblances with some of the published work that we have mentioned in the introduction.[5–8]

Apart from this effect, we observe a small blue-shift of the luminescence peaks (less than 2 nm), in the undoped sample, in contrast to the very strong change of the luminescence bands observed in the doped sample: their spectral width is dramatically reduced, and also a noticeable blue-shift takes place. We noticed in addition that the blue-shift on the undoped sample is more important when measured

with CL than with PL, due to the different excitation conditions. Taking into account our preliminary study on the as-grown samples, we analyze the observation for the doped sample as evidence that the $SiCl_4/H_2/Ar$ plasma has an effect on the built-in electric field initially present in the sample. The electric field is reduced on the whole thickness of the QW structure, although the etching has affected only 250 nm on the top surface. Reducing the electric field reduces the QCSE which impacts QW 1 to QW 8 in this sample. According to the CL result, the charge carrier escape from QW 9, which is an effect of the strong electric field in the p-n junction, is also suppressed or reduced by the $SiCl_4/H_2/Ar$ plasma etching. This reduction of the internal electric field in the doped sample can only be the consequence of the penetration of charged species during the plasma exposure. We suggest that these charged species could be Cl^- ions, either directly generated in the plasma or resulting from Cl atoms or excited radicals having captured an electron inside the sample. However, the concentration of these ions is not high enough to be detected on the SIMS profiles. Only the higher Cl concentration immediately beneath the surface is observed on the SIMS profiles.

Finally, we also interpret the blue-shifts on the undoped sample as a reduction of the built-in electric field (weak with respect to the doped sample) present in this sample after growth. The fact that this blue-shift is more important when measured with CL is a consequence of the different excitation schemes for CL and PL.

Then we investigated the Cl_2/N_2 plasma. The etch rate for this plasma is very low under the conditions of our experiment. However, its impact on the undoped sample consists in inducing much larger blue-shifts than the $SiCl_4/H_2/Ar$ plasma: a maximum of 7.2 nm is observed for QW 2. On the contrary, on the doped sample, this plasma produces little effect, only a sharpening of the line for QW 1 and, to a lesser extent, QW 2. No blue-shift is observed on the doped sample. The QCSE is still present in the doped sample after this plasma exposure; it is only reduced very close to the surface. Altogether, this plasma has very little effect on the internal built-in electric field. The explanation for the strong blue-shifts observed on the undoped sample cannot be related to suppression of the QCSE, since a similar suppression or reduction does not take place in the doped sample. SIMS profiles for this plasma indicate, as for the previous plasma, only a limited penetration of Cl beneath the surface.

It seems logical to claim that the different effects observed for the two plasmas would be due, at least in part, to the presence of N in the Cl_2/N_2 plasma. We were not able to measure the N profiles in SIMS; however, it is rather probable that N penetrates the sample under such plasma exposure, since N does not contribute to the etching reactions at the surface. Then, considering the possible penetration of N, we could explain the blue-shifts observed on the undoped sample as a consequence of the interaction between the N atoms and the crystal matrix. The blue-shifts of the PL lines measured enter within the margins expected for a compressive stress of the lattice,[16,17] which would be induced by N interstitials. It is interesting to point the fact that on the PL spectra the QW lines do not show a conspicuous splitting corresponding to the lh and hh related transitions.[18] Actually, we could have anticipated this seeing two different peaks resolved for each QW transition in the as-grown sample (due to the intrinsic stress of the $InAs_xP_{1-x}$ layers). This is not the case, either because the magnitude of the splitting between heavy-hole and light-hole transitions is too small to be resolved experimentally, even for the most strained QW, or because our excitation power density for the PL measurement is not in the adequate range. Even if we do not see the splitting on the as grown sample, the mechanical stress induced by the N atoms interacting with the structure could create the splitting if this stress occurs in a biaxial geometry. We suggest that the presence of N, in an interstitial position, mainly induces a hydrostatic stress which does not change the symmetry of the PL transitions observed, since hydrostatic stress does not split the lh and hh related bands. The magnitude of the blue-shifts for the different QWs is dependent from their position. A maximum is recorded for QW 2 with a PL peak blue-shifted by 7.2 nm. Then, a decrease of the blue-shift is observed for the deeper QWs. This variable blue-shift could be attributed to the combination of the effect of interstitial N with the native compressive biaxial stress related to As incorporation changing in the different QWs. However, further investigations would be required to confirm this hypothesis.

On the other hand, we did not observe the blue-shifts in the case of the doped sample. This sample is strongly affected by the QCSE, which is not suppressed nor even reduced for most of the structure by the Cl_2/N_2 plasma etching. Actually, we have no exact idea of the scenario resulting from combined QCSE and compressive hydrostatic stress, but certainly, the QCSE might dominate masking the observation of the blue-shifts due to stress.

Finally, let us consider the $SiCl_4/Ar$ plasma experiments, which were designed to test the effects of the etch rate under conditions of constant reactive gas injection. For the very slow etch process, we observed a maximum penetration of the Cl in the structure, with a distribution similar to that resulting from an implantation mechanism. On the other hand, very few changes appeared on the CL spectrum after this slow etching plasma. Only a slight modification of the electric field close to the surface may occur, explaining the alone change of QW 1 related emission, while the emission from the other QWs did not show significant changes. The association of these trends (maximum penetration of Cl, limited change on the CL spectrum) points to the fact that probably the Cl species penetrating the sample is now atomic Cl, contrary to what we claim for the $SiCl_4/H_2/Ar$ plasma. For the fast etching process, we observe a much more limited penetration of Cl than for the slow etching process. The CL spectrum is more strongly affected, suggesting the presence of Cl^- ions, rather than neutral Cl atoms.

From these combined observations, we now try to build up a scheme for the interaction mechanisms of the etching plasma and the QWs structure, at least for the $SiCl_4/Ar$ plasma:

(1) different forms of Cl play a relevant role in this mechanism, at least Cl^- and atomic Cl;

Author Proof

(2) only the Cl present at the surface contributes to the etching process, while the Cl penetrating across the surface inside the sample does not contribute to the etching process;
(3) the etching experiments with $SiCl_4$/Ar plasmas give a conspicuous anticorrelation between the amount of Cl inside the sample and the etching rate.

In order to quantify this last point, the SIMS data were also exploited to identify a possible trend on the concentration on Cl at the surface at the different steps of the etching process. The signal measured for ^{35}Cl for the first point recorded (sputter time 5.4×10^{-1} s/sputter depth approximately 2.5 nm) was used as an indication of the Cl level at the surface before performing the sputter profile. This is shown in Table III ("Surface Cl"). This analysis was carried out for all the SIMS profiles measured, and Table III indicates also the corresponding etching rate. These data show that the surface Cl signal is between 1.84 and 6.15×10^5 counts/s for the as-grown surfaces and for the surfaces of samples exposed to plasmas with a fast etching rate, while for samples exposed to plasmas with a slow etching rate the Cl surface signal measured lies between 3.89 and 5.26×10^6 counts/s, i.e., approximately an order of magnitude higher. Concerning the bulk Cl concentration, one observes that for the lowest etching rate, especially for the sample exposed to the $SiCl_4$/Ar plasma "slow etch rate," the bulk Cl signal displays a maximum value.

Therefore, the tendency derived from the SIMS data is that the high etch rates are observed for samples that display the smaller Cl signal at both the surface and the bulk, while the slow etch rates are observed when the Cl signal is high at both the surface and the bulk. This suggests that the Cl species that are active in the etching process do not penetrate inside the samples, whereas the forms that penetrate inside the samples are inefficient for the etching process. Figure 19 illustrates in more details this tendency observed for the different etch plasmas investigated.

V. SUMMARY AND CONCLUSIONS

The experimental work detailed in this paper is based on the long-established methodology of dedicated QW structure for the investigation of defect production and consequences during plasma etching of III–V semiconductor materials. Using a combination of characterization techniques, including PL, CL, SIMS, and TEM, we tried to quantify the effects

TABLE III. SIMS data for Cl at the surface and etch rate. The surface data are taken as the SIMS count for the first point recorded (after 5.4×10^{-1} s sputtering).

No.	Sample description	Surface Cl (counts/s)	Etch rate
1	As-grown sample	1.84×10^5	—
2	$SiCl_4/H_2$/Ar —1 min	4.13×10^5	250–300 nm/min
3	Cl_2/N_2—1 min	3.89×10^6	60 nm/min
4	As-grown sample	6.15×10^5	—
5	$SiCl_4$/Ar plasma—slow (1 min)	5.26×10^6	55 nm/min
6	$SiCl_4$/Ar plasma—fast (1 min)	5.81×10^5	400 nm/min

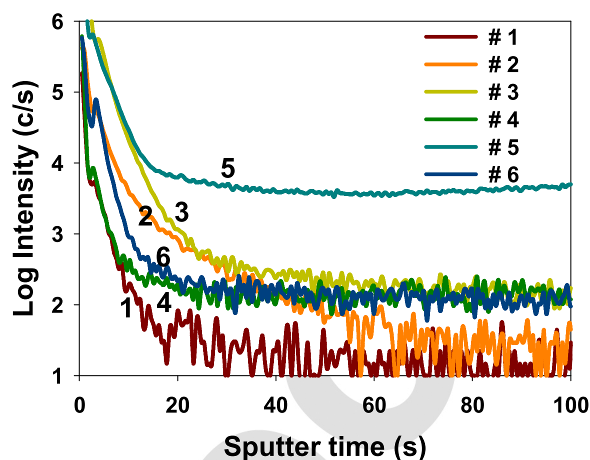

FIG. 19. (Color online) SIMS profiles measured for the different samples displayed in Table III, in log scale, for the early stages of the sputter process between 0 and 100 s.

of different plasma etching chemistries used in the context of fabrication of InP-based photonic circuits. These chemistries have in common the fact that they involve chlorine compounds.

We first analyzed carefully the properties of the "as-grown" samples (before any plasma exposure), observing the importance of taking into account the type and amount of doping in the samples. Indeed, doping is associated with the presence of a built-in electric field whose impact on the luminescence spectra can be very significant, through the quantum confined Stark effect, and also the fact that generated carriers can escape from the QWs through tunneling induced by this built-in electric field. Having understood why the luminescence spectra differ in samples with different doping profiles, we could perform a systematic study of different etching chemistries. The first chemistry ($SiCl_4/H_2$/Ar) yields an etch rate in the order of 250–300 nm/min in our conditions, which is interesting when trying to etch features several micrometers deep. We have limited the exposures to very short durations (1 and 2 min) to avoid etching the whole QW structure. The luminescence of the QWs closest to the etch front was observed to decrease and disappear, similar to previous results in the literature; however, this is the case only for the first and probably second QW, and the deeper QWs are not affected. The other observation is a very significant difference between the undoped and the doped samples: in the case of the undoped sample, no change of the spectral shape for the remaining luminescence peaks occurs, while for the doped sample a very pronounced spectral sharpening is seen. The two types of sample react differently to the plasma. We tentatively explain this difference suggesting that some of the Cl species from the plasma penetrate through the QW structure (which is confirmed by the SIMS profiles), and that part of these species bares an electric charge (probably Cl^- ions). Thus, they modify the built-in electric field in a way for which the QCSE and associated carrier escape are reduced.

This effect—sharpening of the luminescence peaks—is much less pronounced in the case of the Cl_2/N_2 plasmas,

ID: aipepub3b2server Time: 16:08 I Path: D:/AIP/Support/XML_Signal_Tmp/AI-JVA#160068

which anyhow display a reduced etch rate (60 nm/min). The main effect of these plasmas is a blue-shift of the luminescence peaks (especially observable on the undoped sample), which we attribute to the penetration of N in the QW structure. N occupies interstitial sites, thus producing a hydrostatic compressive stress.

Finally, we also investigated a $SiCl_4$/Ar chemistry, for which we were able to vary the etch rate between 55 and 400 nm/min keeping the flow rates constant (i.e., the "chemistry" constant). This last experiment, apart from confirming the spectral sharpening effect observed with the $SiCl_4/H_2$/Ar chemistry, leads us to suggest a balance mechanism for the interplay between the Cl-species active for the etching process at the surface, and the Cl-species that penetrate the sample structure and are "lost" for the etching process, lowering the etching efficiency. From our observations, a tendency appeared for the etch rate to be anticorrelated to the amount of Cl-species present beneath the surface (as detected by the SIMS profiles).

All the results described in this paper point to the importance of checking the impact of reactive etching plasmas on the remaining materials structures. Even though our experiments were performed in the absence of any mask structure, we can claim that when using similar plasmas for the production of photonic features with a three-dimensional geometry (like a simple rectangular ridge structure), similar effects would occur due to the LATERAL penetration of the etching species through the structures being etched, producing the same artifacts that we have described. Taking into account these possible artifacts in the general design of photonic devices is an issue that cannot be neglected. Thanks to the lateral resolution of the CL technique, which we have not used in the present study, we will be able to extend our general methodology to the case where quantifying etching-induced defects within 3D structures (e.g., rectangular waveguides) is required. This will be the next step of this study.

ACKNOWLEDGMENTS

Thomas Delhaye (University Rennes-1) is acknowledged for the SIMS measurements. J. Jimenez and A. Torres were funded by Junta de Castilla y León (Project No. VA293U13).

[1] D. Borah *et al.*, J. Phys. D: Appl. Phys. **44**, 174012 (2011).
[2] B. Wu, A. Kumar, and S. Pamarthy, J. Appl. Phys. **108**, 051101 (2010).
[3] V. M. Donnelly and A. Kornblit, J. Vac. Sci. Technol., A **31**, 050825 (2013).
[4] D. L. Green, E. L. Hu, P. M. Petroff, V. Liberman, M. Nooney, and R. Martin, J. Vac. Sci. Technol., B **11**, 2249 (1993).
[5] C.-H. Chen, D. G. Yu, E. L. Hu, and P. M. Petroff, J. Vac. Sci. Technol., B **14**, 3684 (1996).
[6] R. Germann, A. Forchel, M. Bresch, and H. P. Meier, J. Vac. Sci. Technol., B **7**, 1475 (1989).
[7] M. Rahman, L. G. Deng, C. D. W. Wilkinson, and J. A. van den Berg, J. Appl. Phys. **89**, 2096 (2001).
[8] H. F. Winters, D. B. Graves, D. Humbird, and S. Tougaard, J. Vac. Sci. Technol., A **25**, 96 (2007).
[9] J. P. Landesman *et al.*, Microelectron. Reliab. **55**, 1750 (2015).
[10] J. W. Lee, C. R. Abernathy, S. J. Pearton, C. Constantine, R. J. Shul, and W. S. Hobson, Plasma Sources Sci. Technol. **6**, 499 (1997).
[11] J.-M. Bonard, J.-D. Ganière, B. Akamatsu, D. Araújo, and F.-K. Reinhart, J. Appl. Phys. **79**, 8693 (1996).
[12] S. J. Pennycook, B. Rafferty, and P. D. Nellist, Microsc. Microanal. **6**, 343 (2000). AQ2
[13] L. Viña, E. E. Mendez, W. I. Wang, L. L. Chang, and L. Esaki, J. Phys. C: Solid State **20**, 2803 (1987).
[14] D. Gallet, G. Hollinger, C. Santinelli, and L. Goldstein, J. Vac. Sci. Technol., B **10**, 1267 (1992).
[15] R. Chanson, A. Rhallabi, C. Cardinaud, M. C. Fernandez, and J. P. Landesman, J. Vac. Sci. Technol., A **31**, 011301 (2013).
[16] S. Zemon, S. K. Shastry, P. Norris, C. Jagannath, and G. Lambert, Solid State Commun. **58**, 457 (1986).
[17] O. Martínez, L. F. Sanz, J. Jiménez, A. Martín-Martín, B. Gérard, and E. Gil-Lafon, J. Appl. Phys. **101**, 054901 (2007).
[18] E. Yablonovitch and E. O. Kane, J. Lightwave Technol. **6**, 1292 (1988).

Author Proof